Sub-four-cycle laser pulses directly from a high-repetition-rate optical parametric chirped-pulse amplifier at 3.4 μm

B. W. Mayer,[1,*] C. R. Phillips,[1,2] L. Gallmann,[1] M. M. Fejer,[2] and U. Keller[1]

[1]*Department of Physics, Institute for Quantum Electronics, ETH Zurich, Zurich 8093, Switzerland*

[2]*Edward L. Ginzton Laboratory, Stanford University, Stanford, California 94305, USA*

**Corresponding author: mayerb@phys.ethz.ch*

Received August 15, 2013; revised September 18, 2013; accepted September 18, 2013; posted September 19, 2013 (Doc. ID 195882); published October 16, 2013

We generate sub-four-cycle pulses (41.6 fs) with 12 μJ of pulse energy in the mid-infrared spectral range (center wavelength 3.4 μm) from a high-repetition-rate, collinear three-stage optical parametric chirped-pulse amplifier (OPCPA) operating at 50 kHz. Apodized aperiodically poled MgO:$LiNbO_3$ crystals with a negative chirp rate are employed as gain media to achieve ultrabroadband phase-matching while minimizing optical parametric generation. The seed pulses are obtained via a 1.56 μm femtosecond fiber laser, which is spectrally broadened in a dispersion-shifted telecom fiber to support 1000 nm bandwidth idler pulses in the mid-infrared.

OCIS codes: (140.0140) Lasers and laser optics; (190.4970) Parametric oscillators and amplifiers; (190.7110) Ultrafast nonlinear optics.

http://dx.doi.org/10.1364/OL.38.004265

Recent developments in the generation of higher-order harmonics (HHG) show a clear trend towards the application of coherent and bright light sources operating at long wavelengths, enabling the generation of XUV- or multi-hundred-electron volt (eV) and even kiloelectron volt (keV) soft x-ray pulses [1,2]. Long-wavelength ultrashort laser pulses thus enable new capabilities for multidimensional spectroscopy and studies on atomic and molecular dynamics [3–6], in both the mid-infrared and XUV regions. To achieve high signal-to-noise ratios in the sensitive detection schemes used for many applications, light sources with high average photon flux are needed. In particular, higher repetition rates than those of conventional Ti:sapphire-based systems (which mainly operate in the few-kilohertz regime) are strongly favored. The development of suitable optical parametric amplifier (OPA)- and optical parametric chirped-pulse amplifier (OPCPA)-based sources is progressing rapidly, with reported systems operating at central wavelengths near 1.8 μm [7–9], 2 μm [10–12], 3 μm [13,14], 3.4 μm [15,16], and 4 μm [17].

In this Letter, we present a collinear, high-repetition-rate, mid-infrared OPCPA system operating at a center wavelength of 3.4 μm based on aperiodically poled lithium niobate (APPLN) OPA devices. The collinear interaction in such quasi-phase-matching (QPM) devices in contrast to noncollinear phase-matching in bulk crystals gives an idler output without an angular chirp. Compared with our previous work [16], this new system has been fully redesigned to account for recent developments in the theory of these devices [18,19], and to suppress parasitic spatial effects [20]. The new system design solves the seed bandwidth limitations of our previous system [16], greatly reduces optical parametric generation (OPG), and maintains good quantum conversion efficiency (≈24.5%) of the final OPA stage.

The new system delivers sub-four-cycle pulses [41.6 fs full width at half-maximum (FWHM)], without being limited by the damage threshold of the gain crystals, or by the bandwidth of the seed pulses provided by our fiber laser (in contrast to our previous result [16]). In particular, we show for the first time, to the best of our knowledge, the bandwidth capabilities of aperiodically poled MgO:$LiNbO_3$ amplification devices by demonstrating 1000-nm-wide gain while maintaining compressible output idler pulses.

In such aperiodic (or chirped) QPM gratings, the grating k vector is swept smoothly and monotonically through phase-matching for all of the spectral components of interest. Signal and idler spectral components experience gain in the vicinity of their local phase-matching points. A unique aspect of this approach to OPCPA is that the gratings can support almost arbitrary phase-matching bandwidths with the potential for customized gain profiles [21,22], good conversion efficiencies [18,23], and access to bandwidths beyond those possible with conventional birefringent phase-matching techniques without operating at the crystal damage threshold. Furthermore, the system complexity is kept at a minimum by the collinear nature of the OPCPA chain. These properties make our approach an excellent route towards relatively compact systems offering intense few-cycle mid-infrared pulses for attosecond science.

Our OPCPA system is shown schematically in Fig. 1. We first generate a broadband seed source around

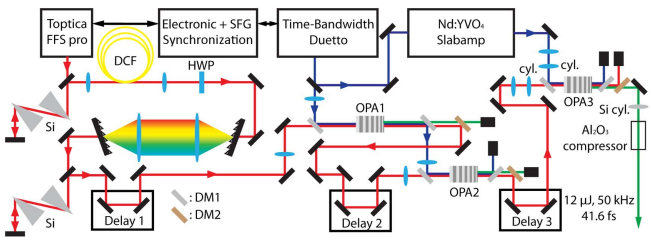

Fig. 1. Schematic overview of the mid-infrared OPCPA setup. DM, dichroic mirror; DM1, reflective 1064 nm/transmissive 1560 and 3400 nm; DM2, reflective 1560 nm/transmissive 3400 nm.

1.56 μm, amplify this pulse in the OPCPA chain, and extract the generated idler pulse after the final OPCPA stage. As the primary seed source for the system, we use a mode-locked femtosecond fiber laser operating at $\lambda = 1.56$ μm with a bandwidth corresponding to 65-fs transform limited pulse energy of 3.1 nJ at 80 MHz repetition rate (250 mW average power). Since our goal is to generate few-cycle infrared idler pulses, we first need to generate the required seed bandwidth in the near-infrared spectral range before seeding the OPCPA system. For this purpose, the pulses are first compressed to their transform limit via a pair of silicon prisms in a double-pass configuration. For our new spectral broadening system, the pulses are collimated with a pair of standard lenses and then coupled into a 1-m-long dispersion-shifted (DS) telecom fiber (DCF3, Thorlabs Inc.) with a zero-dispersion wavelength of ≈1.6 μm. This fiber operates in the normal dispersion regime, in contrast to the anomalous dispersion regime, which can be utilized for soliton pulse compression. The initially compressed input pulse is thus spectrally broadened while it is temporally dispersed through the fiber. This configuration avoids the modulation instability regime while still utilizing convenient off-the-shelf telecom fiber technology.

At the output of the spectral broadening fiber, the seed pulse supports more than 250 nm of signal bandwidth. To provide an OPCPA seed, the polarization of the spectrally broadened pulse is optimized with a half-wave plate (HWP) and then stretched by a 4f pulse shaper in a double-pass configuration. The pulse shaper consists of two metallic plane folding mirrors, two plane-concave cylindrical mirrors with a radius of curvature (ROC) of −800 mm, and two holographic transmission gratings with 600 lines/mm. The gratings exhibit a single-pass efficiency of greater than 85% at the design wavelength of 1.55 μm. A double-pass configuration of a subsequently arranged pair of silicon prisms provides the third-order dispersion (TOD) required to compress the final output pulses.

The spectrum after the 4f pulse shaper and the pair of silicon prisms is shown in Fig. 2(a) ("seed" curve, black solid line). The pulse energy available to seed the first OPCPA stage (depicted as OPA1 in Fig. 1) is 92.5 pJ. The spectral ripples seen in Fig. 2(a) originate from the imperfect pulse profile used to seed the DS fiber: while spectral broadening in the positive dispersion regime can in principle provide smooth output spectra, in our case, the pulses are already partially distorted by the nonlinear broadening that also occurs in the erbium-doped fiber amplifiers (EDFAs) of the fiber laser system itself. We confirmed this conclusion via numerical modeling of the spectral broadening process in the DS fiber using standard techniques [24,25], assuming the frequency resolved optical gating (FROG)- reconstructed pulses emitted by the fiber laser as input to the model. During the OPA process, any modulations of the seed spectrum are transferred to the generated idler spectrum.

The primary pump source for our OPCPA system is an industrial laser (Time-Bandwidth-Products Inc., Duetto) operating at 1.064 μm and delivering 12 ps pulses at a repetition rate of 50 kHz and average output power of up to 10 W. The output of this laser is split in two parts. One part is further amplified by a Nd:YVO_4 Innoslab-type amplifier [26], to provide a higher-power pump for the final OPA stage. The remaining part is collinearly overlapped with the seed in OPA1 via a dichroic mirror, denoted DM1 in Fig. 1 (transmissive for the seed at 1560 nm and reflective for the pump at 1064 nm). The average pump power reaching OPA1 is 5.7 W (113 μJ), and it is focused to a spot size of 315 μm ($1/e^2$ radius), corresponding to an intensity of 4.9 GW/cm^2. The pump output after the uncoated OPA1 crystal is split from the signal and idler outputs by another dichroic mirror DM1. In the new layout of our OPCPA chain, this pump is then reused to seed OPA2, providing a power of 3.8 W. The pump is refocused in OPA2 to an intensity of 6.7 GW/cm^2 ($1/e^2$ radius of 220 μm) and collinearly overlapped with the signal output of OPA1 (~1.56 μm), which is split from the idler by dichroic mirror DM2 after the first amplification stage. The gain of the preamplification part of the system (i.e., between the OPA1 input and the OPA3 input) corresponds to 42.8 dB.

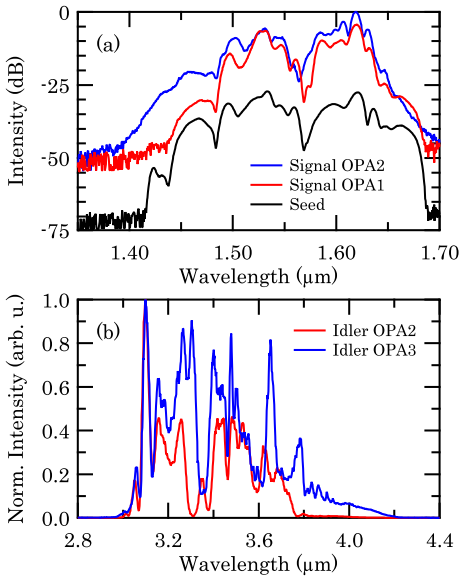

Fig. 2. (a) Signal spectra. Spectra of the seed (black line) and the amplified signal after OPA1 and OPA2, respectively (red and blue lines). An offset has been added to the seed curve for clarity. (b) Normalized mid-infrared idler spectra after OPA2 (red) and OPA3 (blue), respectively.

The spectra of the seed and the amplified signals are shown in Fig. 2(a). Note that the amplified spectra also contain the unamplified 80 MHz background from the seed source. With respect to these spectra, there is evidence of gain narrowing, due to the non-flat-top pump temporal profile, reducing the amplification for signal spectral components below 1.475 μm and above 1.625 μm.

The third and final amplification stage, denoted OPA3, is pumped by the output of our Innoslab amplifier [26]. The pump power reaching the OPA3 crystal is 15.2 W, corresponding to 304 μJ. The signal output of OPA2 is used as the seed for this stage, and the generated mid-infrared idler around $\lambda = 3.4$ μm is extracted afterwards as the final output of the system. Dichroic mirrors DM1 and DM2 are used to combine and split up the waves.

In OPA3, we use a moderate peak intensity of the pump so as to not drive the crystal too strongly. A consequence

of pumping the crystal too strongly is the onset of beam fanning, likely due to photorefractive effects driven by parasitic green light, which is generated primarily due to random duty cycle variations in the QPM grating [19]. To use all of the available pump power in the 1-mm-aperture APPLN devices, we use elliptical foci for the pump and signal beams. To obtain the required beam sizes, we employ both spherical and cylindrical lenses (indicated by "cyl." in Fig. 1), forming one spherical and one cylindrical telescope. The pump beam is focused to an intensity of 4.4 GW/cm^2 ($1/e^2$ width of 700 μm in the horizontal dimension corresponding to the direction of the crystal c axis, $1/e^2$ width of 1700 μm in the vertical dimension). The resulting idler spectra of OPA2 and OPA3 are shown in Fig. 2(b). The spectra are measured with an imaging grating spectrometer.

In all stages we use newly designed uncoated MgO:LiNbO$_3$ crystals, each having an 11-mm long, 1-mm by 3-mm wide, apodized APPLN grating design with a chirp rate of $\kappa = -2.5$ mm^{-2} (corresponding to a decreasing period versus position) in order to achieve a broad phase-matching in a spectral window spanning the 3 to 4 μm spectral range. Concerning apodization, we have studied the importance of apodization profiles for such chirped QPM devices experimentally [27], and have recently shown how they can be implemented systematically for a wide range of parametric interactions [18].

For idler compression after OPA3, we utilize propagation through a bulk medium. Our compressor consists of a 50-mm long rod of coated sapphire, with the length chosen as a trade-off between efficiency and gain narrowing in the preamplifier OPCPA stages. Note that adjustment of the dispersion compensation primarily takes place on the seed pulse in the near-infrared spectral range. Due to the phase-reversal properties of OPA, the even-order spectral phase components of the idler inherit, approximately, the even-order components of the seed spectral phase with a flipped sign, whereas the sign of odd-order components of the idler phase is not flipped [21]. The combination of the applied seed phase, which utilizes the 4f pulse shaper and pair of silicon prisms described above, and idler propagation through the bulk sapphire after the final OPA stage enables compensation of the idler spectral phase up to fourth order. With this approach, we were able to compress the chirped 3.4 μm pulses to 41.6 fs (sub-four-cycles), with 12 μJ of pulse energy after collimation and compression. The compressed pulses were characterized with mid-infrared second-harmonic generation (SHG)-FROG, as shown in Fig. 3. With respect to the retrieved spectrum, we believe the discrepancy compared to the measured spectrum originates from the spectral dependence of SHG conversion efficiency and beamsplitter characteristics over the large bandwidth supported by the idler spectrum. However, the 68.8 fs FWHM of the autocorrelation signal provides additional evidence for the sub-four-cycle duration of our pulses.

It is important to note that inside the APPLN grating, the generated idler power is approximately 948 mW (≈19 μJ). This value was calculated when accounting for all linear losses encountered from the optical elements after OPA3, including Fresnel losses from the end facet of the uncoated APPLN grating. We estimate a corresponding internal conversion efficiency (number

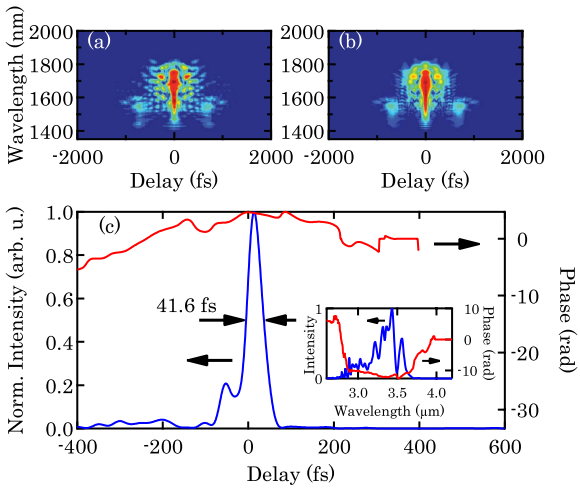

Fig. 3. (a) Measured SHG-FROG spectrogram of the compressed 41.6 fs mid-infrared pulse. The FROG error for a grid size of 512 by 386 points is 0.0116. (b) Retrieved spectrogram and (c) retrieved temporal intensity and phase. The inset shows the retrieved spectrum and spectral phase.

of idler photons at the end of the QPM grating divided by the number of pump photons at the input) of 24.5%. With respect to the overall gain in the system, the net amplification between the OPA3 input and compressor output corresponds to 11.8 dB.

In order to develop a working OPCPA system using APPLN devices, several important design constraints must be met that go beyond using QPM gratings to support a sufficient phase-matching bandwidth. For example, with a given phase-matching bandwidth and OPA gain, the noncollinear gain guided modes discussed in [20] can be fully suppressed with a sufficient pump peak power, thereby suppressing excess OPG. By the design of the system layout and the APPLN gratings, the presence of OPG has been minimized. Specifically, by operating our system at 50 kHz and reusing the OPA1 transmitted pump for OPA2, we are able to satisfy this pump peak power constraint in each stage, and also ensure sufficient seed power for OPA3 without excessively saturating OPA1 and OPA2.

The remaining OPG background was characterized first by measuring the idler output power while operating the amplification chain in an unseeded configuration and also by a spectral characterization of the OPG. The spectra of the amplified idler (seeded case) and the OPG (unseeded case) are shown in Fig. 4. Note the different scales for the idler spectrum of OPA3 and the idler OPG spectrum. In both cases the amount of amplified quantum noise accounts for less than 2.5% of the total idler power, and this value represents an overestimate of the actual OPG in the seeded system. This value is a substantial improvement compared to the background in our previous OPCPA system [16] and to reported OPG levels of other comparable systems [10–12]. To the best of our knowledge, this is the lowest OPG background within output pulses delivered by a high-repetition-rate, mid-infrared OPCPA reported so far, and proves that the excess quantum noise amplification discussed in [20] for this type of gain medium can be fully suppressed by appropriate system design.

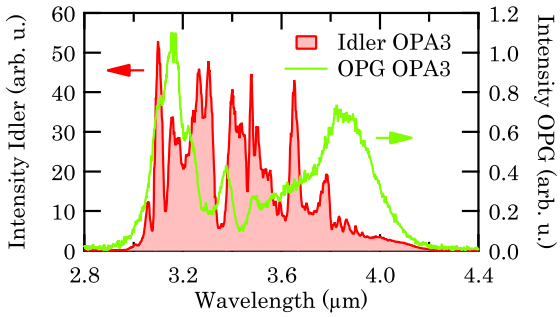

Fig. 4. OPG spectrum for the unseeded case of the amplifier chain in comparison to the idler spectrum of OPA3. Note the different scales for the idler and OPG spectrum. The power contained by the area under the green OPG curve accounts for less than 2.5% of the total amount of idler power.

In addition to redesigning the OPCPA stages to minimize OPG while improving bandwidth and maintaining conversion efficiency, the sign of the pulse chirp was also flipped (we now use a sapphire compressor instead of a silicon compressor [16]). This change was made in order to optimize the OPCPA temporal dynamics. Furthermore, in addition to being more convenient experimentally, seeding the power amplifier stage (OPA3) with the signal rather than the idler helps to suppress unwanted processes such as idler SHG. The details of this and other subtle aspects of our system design are beyond the scope of this Letter, and will be discussed further in future work.

In conclusion, we have demonstrated a 50 kHz, mid-infrared light source delivering 41.6 fs record-short pulses directly from such a high-repetition-rate OPCPA at 3.4 μm central wavelength. The system provides a compressed pulse energy of 12 μJ. Additionally, good internal conversion efficiency of 24.5% was achieved and the OPG background was minimized by the redesign of the seeding and amplification scheme. The internal conversion efficiency is an indication that the power amplifier stage OPA3 is operating in a strongly saturated regime, with the potential to eventually access the fully saturated adiabatic frequency conversion limit [18]. So far, we are using 1-mm by 3-mm wide APPLN gratings. In recent years, wide-aperture samples have become available [28], allowing QPM technology to support very high energies. In combination with new developments in high-power ultrafast amplifiers [29,30], this technology should enable high-power and high-repetition-rate few-cycle pulse generation in the mid-infrared.

This research was supported by the Swiss National Science Foundation (SNSF) through grant no. 200020_144365/1, and by a Marie Curie International Incoming Fellowship within the 7th European Community Framework Programme. M. M. Fejer acknowledges support of the U.S. Air Force Office of Scientific Research (AFOSR).

References

1. C. Trallero-Herrero, C. Jin, B. E. Schmidt, A. D. Shiner, J.-C. Kieffer, P. B. Corkum, D. M. Villeneuve, C. D. Lin, F. Légaré, and A. A. T. Le, J. Phys. B **45**, 011001 (2012).
2. T. Popmintchev, M.-C. Chen, D. Popmintchev, P. Arpin, S. Brown, S. Ališauskas, G. Andriukaitis, T. Balčiunas, O. D. Mücke, A. Pugzlys, A. Baltuška, B. Shim, S. E. Schrauth, A. Gaeta, C. Hernández-García, L. Plaja, A. Becker, A. Jaron-Becker, M. M. Murnane, and H. C. Kapteyn, Science **336**, 1287 (2012).
3. C. T. Middleton, P. Marek, P. Cao, C.-C. Chiu, S. Singh, A. M. Woys, J. J. de Pablo, D. P. Raleigh, and M. T. Zanni, Nat. Chem. **4**, 355 (2012).
4. M. Yang, Ł. Szyc, J. Dreyer, E. T. J. Nibbering, and T. Elsaesser, J. Phys. Chem. A **114**, 12195 (2010).
5. P. Hamm and M. T. Zanni, *Concepts and Methods of 2D Infrared Spectroscopy* (Cambridge University, 2011).
6. P. Colosimo, G. Doumy, C. I. Blaga, J. Wheeler, C. Hauri, F. Catoire, J. Tate, R. Chirla, A. M. March, G. G. Paulus, H. G. Muller, P. Agostini, and L. F. DiMauro, Nat. Phys. **4**, 386 (2008).
7. C. Li, D. Wang, L. Song, J. Liu, P. Liu, C. Xu, Y. Leng, R. Li, and Z. Xu, Opt. Express **19**, 6783 (2011).
8. B. E. Schmidt, A. D. Shiner, P. Lassonde, J.-C. Kieffer, P. B. Corkum, D. M. Villeneuve, and F. Légaré, Opt. Express **19**, 6858 (2011).
9. M. Bradler, C. Homann, and E. Riedle, "Broadband difference frequency mixing between visible and near-infrared pulses for few-cycle pulse generation with stable carrier-envelope phase," Appl. Phys. B (to be published).
10. T. Fuji, N. Ishii, C. Y. Teisset, X. Gu, T. Metzger, A. Baltuška, N. Forget, D. Kaplan, A. Galvanauskas, and F. Krausz, Opt. Lett. **31**, 1103 (2006).
11. X. Gu, G. Marcus, Y. Deng, T. Metzger, C. Teisset, N. Ishii, T. Fuji, A. Baltuska, R. Butkus, V. Pervak, H. Ishizuki, T. Taira, T. Kobayashi, R. Kienberger, and F. Krausz, Opt. Express **17**, 62 (2009).
12. Y. Deng, A. Schwarz, H. Fattahi, M. Ueffing, X. Gu, M. Ossiander, T. Metzger, V. Pervak, H. Ishizuki, T. Taira, T. Kobayashi, G. Marcus, F. Krausz, R. Kienberger, and N. Karpowicz, Opt. Lett. **37**, 4973 (2012).
13. C. J. Fecko, J. J. Loparo, and A. Tokmakoff, Opt. Commun. **241**, 521 (2004).
14. M. Hemmer, A. Thai, M. Baudisch, H. Ishizuki, T. Taira, and J. Biegert, Chin. Opt. Lett. **11**, 013202 (2013).
15. C. Heese, C. R. Phillips, L. Gallmann, M. M. Fejer, and U. Keller, Opt. Lett. **35**, 2340 (2010).
16. C. Heese, C. R. Phillips, B. W. Mayer, L. Gallmann, M. M. Fejer, and U. Keller, Opt. Express **20**, 26888 (2012).
17. G. Andriukaitis, T. Balciunas, S. Alisauskas, A. Pugzlys, A. Baltuska, T. Popmintchev, M.-C. Chen, M. M. Murnane, and H. C. Kapteyn, Opt. Lett. **36**, 2755 (2011).
18. C. R. Phillips, C. Langrock, D. Chang, Y. W. Lin, L. Gallmann, and M. M. Fejer, J. Opt. Soc. Am. B **30**, 1551 (2013).
19. C. R. Phillips, J. S. Pelc, and M. M. Fejer, J. Opt. Soc. Am. B **30**, 982 (2013).
20. M. Charbonneau-Lefort, B. Afeyan, and M. M. Fejer, J. Opt. Soc. Am. B **25**, 1402 (2008).
21. M. Charbonneau-Lefort, B. Afeyan, and M. M. Fejer, J. Opt. Soc. Am. B **25**, 463 (2008).
22. C. R. Phillips, L. Gallmann, and M. M. Fejer, Opt. Express **21**, 10139 (2013).
23. G. Porat and A. Arie, J. Opt. Soc. Am. B **30**, 1342 (2013).
24. J. M. Dudley, G. Genty, and S. Coen, Rev. Mod. Phys. **78**, 1135 (2006).
25. C. R. Phillips, C. Langrock, J. S. Pelc, M. M. Fejer, I. Hartl, and M. E. Fermann, Opt. Express **19**, 18754 (2011).
26. C. Heese, A. E. Oehler, L. Gallmann, and U. Keller, Appl. Phys. B **103**, 5 (2011).
27. C. Heese, C. R. Phillips, L. Gallmann, M. M. Fejer, and U. Keller, Opt. Express **20**, 18066 (2012).
28. H. Ishizuki and T. Taira, Opt. Express **20**, 20002 (2012).
29. P. Russbueldt, T. Mans, J. Weitenberg, H. D. Hoffmann, and R. Poprawe, Opt. Lett. **35**, 4169 (2010).
30. T. Eidam, S. Hanf, E. Seise, T. V. Andersen, T. Gabler, C. Wirth, T. Schreiber, J. Limpert, and A. Tünnermann, Opt. Lett. **35**, 94 (2010).